Low-Level Wind Maxima and Structure of the Stably Stratified Boundary Layer in the Coastal Zone

Citation	Mahrt, L., Vickers, D., & Andreas, E. L. (2014). Low-Level Wind Maxima and Structure of the Stably Stratified Boundary Layer in the Coastal Zone. Journal of Applied Meteorology and Climatology, 53(2), 363-376. doi:10.1175/JAMC-D-13-0170.1
DOI	10.1175/JAMC-D-13-0170.1
Publisher	American Meteorological Society
Version	Version of Record
Terms of Use	http://cdss.library.oregonstate.edu/sa-termsofuse

Low-Level Wind Maxima and Structure of the Stably Stratified Boundary Layer in the Coastal Zone

L. MAHRT

NorthWest Research Associates, Redmond, Washington

DEAN VICKERS

College of Earth, Ocean, and Atmospheric Sciences, Oregon State University, Corvallis, Oregon

EDGAR L ANDREAS

NorthWest Research Associates, Inc., Lebanon, New Hampshire

(Manuscript received 21 May 2013, in final form 12 October 2013)

ABSTRACT

A Rutan Aircraft Factory Long-EZ aircraft flew numerous low-level slant soundings on two summer days in 2001 off the northeastern coast of the United States. The soundings are analyzed here to study the nonstationary vertical structure of the wind, temperature, and turbulence. An error analysis indicates that fluxes computed from the aircraft slant soundings are unreliable. The first day is characterized by a weakly stable boundary layer in onshore flow capped by an inversion. A low-level wind maximum formed at about 100 m above the sea surface. The second day is characterized by stronger stability due to advection of warm air from the upwind land surface. On this more stable day, the wind maxima are very sharp and the speed and height of the wind maxima increase with distance from the coast. Although trends in the vertical structure are weak, variations between subsequent soundings are large on time scales of tens of minutes or less. The vertical structure of the wind and turbulence is considerably more nonstationary than the temperature structure, although the existence of the wind maximum is persistent. Causes of the wind maxima and their variability are examined but are not completely resolved.

1. Introduction

The marine boundary layer in the coastal zone is frequented by low-level wind maxima that are due to various causes. Baroclinity resulting from land–sea temperature contrasts, sea surface temperature (SST) variations, and the slope of the marine capping inversion can all lead to low-level wind maxima (Zemba and Friehe 1987; Ström and Tjernström 2004; Colle and Novak 2010). Barrier winds and other topographical effects (Ström and Tjernström 2004; Muñoz and Garreaud 2005) may induce low-level jets through horizontal convergence and attendant pressure adjustments. The irregularity of the coastline also affects such wind maxima (Colle and Novak 2010; Angevine et al. 2006; Pichugina et al. 2012; Rahn and Parish 2010), as do changing synoptic-scale patterns. Deep vertical oscillations of the wind field in the troposphere (Mayer et al. 2012) can produce wind maxima near the surface as also seen in the observations of Tjernström and Smedman (1993) and others.

In addition, nocturnal jets may form over land and advect over the coastal zone (Angevine et al. 2006). Baroclinically driven jets in the coastal zone are often influenced by inertial effects and distortion of the flow by topography and may be complex (Burk and Thompson 1996). In most circumstances, multiple mechanisms, including diurnal modification, are present (Grisogono et al. 1998; Bielli et al. 2002; Jiang et al. 2010). Even mesoscale models have difficulty simulating these sharp, low-level wind features, however (Tastula et al. 2012).

This study includes offshore flow of warmer air from land, which often leads to formation of a stable internal

Corresponding author address: L. Mahrt, 2171 NW Kari Pl., Corvallis, OR 97330.
E-mail: mahrt@nwra.com

DOI: 10.1175/JAMC-D-13-0170.1

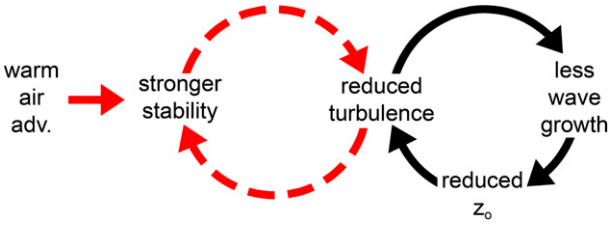

FIG. 1. A sketch of feedback mechanisms with flow of warm air over colder water. The thermal cycle is indicated by the red dashed loop in which warm-air advection and associated stratification suppress the turbulence. The reduced vertical mixing allows more effective stabilizing of the flow. The mechanical cycle is designated by the solid black loop. The reduced turbulence leads to less wave development and smaller surface roughness, which in turn lead to less turbulent mixing. The separation of thermal and mechanical loops is to simplify the conceptual picture. Both loops are fully coupled at all stages.

boundary layer and a wind maximum close to the sea surface. Airflow from land over the less rough sea surface accelerates in response to reduced surface stress. Högström (1984) and Smedman et al. (1993) viewed this acceleration and formation of a low-level jet as an inertial mode resulting from disruption of the force balance in the momentum equation as the offshore flow passes the coast. Consequently, this mechanism is sometimes referred to as the inertial effect, as will be done here. Andreas et al. (2000) evaluated a number of mechanisms responsible for generating low-level jets over sea ice and eliminated all but the inertial mechanism.

Advection of warm air from land over colder water leads to buoyancy destruction of turbulence and restricts the downward mixing of momentum, which in turn reduces the sea surface wave field and surface roughness (Fig. 1). Monin–Obukhov similarity may not apply (Smedman et al. 1995). When the air is significantly warmer than the sea surface and strong stratification seriously limits the turbulence, the decreasing turbulence and decreasing surface roughness evolve together and cause almost complete decoupling of the wind field from the ocean surface (Högström 1984; Smedman et al. 1997a,b; Mahrt et al. 2001a,b; Skyllingstad et al. 2005). The friction velocity decreases well below 0.1 m s^{-1} and the roughness length can decrease below the smooth flow value. This regime is sometimes referred to as quasi-frictional decoupling (Smedman et al. 1997b) or ultrasmooth conditions (Donelan 1990). These cases may correspond to downward transport of turbulence energy (Mahrt et al. 2001b) because the turbulence above the shallow inversion layer is stronger than the very weak turbulence near the surface (Fairall et al. 2006). The accelerating low-level jets and associated strong shear may become dynamically unstable farther downwind, at which point the airflow fully recouples to the sea surface (Smedman et al. 1997a; Mahrt et al. 2001b). Nunalee and Basu (2013) demonstrated the difficulties of modeling coastal jets close to the surface and emphasize the need for more observations.

Flow of air from warm water to cold water across open-ocean SST fronts can also lead to formation of a strong inversion and significant low-level wind maxima, as found in Vihma et al. (1998). Baroclinity associated with the SST variation contributes to the low-level wind maxima in their study. Helmis et al. (2013) recently conducted a case study analysis of three summer days of low-level jets off the east coast of the United States that was based on radiosondes, tower measurements, and remote sensing. They found that warm-air advection, inertial modes, and multiple baroclinic affects, including shallow local baroclinity, could all contribute to the low-level jet. In contrast to the above studies, when the air temperature is only modestly warmer than the sea surface and the flow is sufficiently strong, a cooled, well-mixed layer with a capping inversion forms instead of a strongly stable layer (Lange et al. 2004) and low-level wind maxima are less likely.

This study analyzes a large number of aircraft slant soundings on two days of warm-air advection over cooler water. The first day's flow is onshore and weakly stable, and the second day's flow is offshore with significantly stronger stability.

2. Measurements

We analyze data collected by a Rutan Aircraft Factory Long-EZ aircraft that was operated by T. Crawford during the pilot program of the Coupled Boundary Layers and Air Sea Transfer experiment (CBLAST Weak Wind) conducted over the Atlantic Ocean south of Martha's Vineyard, Massachusetts, during July–August 2001 (Fig. 2). The Long-EZ is a light pusher aircraft with the engine mounted on the rear of the airplane. It has the large main wing set back farther than that of conventional aircraft. The small, low-drag airframe and rear-mounted pusher engine reduce the influence of flow distortion, engine vibration, and engine exhaust for instruments that are mounted on the nose.

Winds are measured using the Best Aircraft Turbulence (BAT) probe (Crawford and Dobosy 1992), positioned 2 m in front of the nose and five wing widths ahead of the canard. Fast-response temperature is measured using a 0.13-mm microbead thermistor mounted inside the design stagnation point port on the BAT hemisphere. The Long-EZ instrumentation is described further in Sun et al. (2001).

FIG. 2. A map of the observational area; n refers to the northern site, and s refers to the southern site.

The radiometrically measured SST is unfortunately not very accurate because of drift of the reference temperature of the Everest Interscience, Inc., 4000.4GL. Absolute errors may be as large as 1°C. Therefore, the radiometer measurements will be used only to qualitatively determine the spatial pattern of the sea surface temperature. Height above the sea surface was measured by a NovAtel, Inc., GPS sensor and calibrated with a Riegl Laser Measurement Systems, GmbH, laser (LD90-3100VHS).

The data were collected at a rate of 50 samples per second with a flight airspeed of about $50\,\mathrm{m\,s^{-1}}$, which corresponds to a horizontal interval of about 1 m between data points. The soundings ascend or descend at a rate of roughly $A \equiv dz/dx \approx 7.5\%$ (where z and x are the vertical and horizontal distances, respectively) with a corresponding height interval of approximately 0.075 m between adjacent data points. Thus, sampling the lowest 150 m corresponds to a horizontal distance of about 2 km. Soundings that do not extend down to 10 m or up to 150 m are discarded.

Horizontal flight legs were flown approximately 10 m above the sea surface. Variations of the sea surface temperature along the flight track are small relative to the roughly 3-K air–sea temperature differences for all three flights examined in this study. The surface heterogeneity of air temperature as based on the horizontal flights is sufficiently weak that small differences in the exact location of the soundings likely lead to insignificant differences between soundings.

This study is based on three of the four flights with the most aircraft soundings. The fourth flight was characterized by weak-wind, stable conditions with chaotic spatial and time variability. The three flights analyzed here are characterized by weak stability, moderate stability, and strong stability. The first flight was carried out during the afternoon of 7 August 2001 and includes 51 soundings in a weakly stable boundary layer, likely maintained by advection of warmer air from warmer water upwind (to the southwest) from the observational site. The second flight was conducted on the morning of 8 August and encountered moderate stability associated with flow of warm air from land over cooler water. At midday, this flight shifted northward by about 25 km, closer to land (Fig. 2), where the stratification was stronger and the wind maximum was lower. A third flight was conducted later in the afternoon of 8 August at the more northerly location. To organize the soundings into more homogeneous groups, the first 20 morning soundings from the second flight at the southern site farthest from land are combined to form the moderately stable group. The 18 early-afternoon soundings at the northern site from the second flight are combined with the 13 soundings from the third flight later in the afternoon to form the ''northern'' group of soundings to represent very stable conditions. We will refer to these three groups of soundings as the weakly stable, moderately stable, and very stable regimes. This grouping is motivated by the much greater spatial variation between the two locations in comparison with the time variability at a given site.

3. Decompositions and error analysis

a. Decomposition

We now examine errors associated with slant soundings in the usual environment with both vertical and horizontal variations. Discussion of errors in aircraft

measurements can be found in Lenschow and Sun (2007) and references therein. Consider an arbitrary variable measured by an aircraft slant sounding at a point in time, $\phi(x, y, z, t)$. Here, $\phi(x, y, z, t)$ will represent potential temperature or one of the three velocity components. The variable $\phi(x, y, z, t)$ can theoretically be decomposed in different ways. We decompose ϕ at a fixed time and point in space as

$$\phi(x,y,z,t) \equiv [\phi](z) + \phi^*(x,y,z,t) + \phi'(x,y,t). \quad (1)$$

Here, $[\phi](z)$ is a horizontal average of ϕ over a relatively large scale whose time variation is neglected, ϕ^* is the spatial deviation of the locally averaged variable from $[\phi]$, and $\phi'(x, y, t)$ is the instantaneous deviation from the local horizontally averaged variable $[\phi] + \phi^*$. In the ideal case, $\phi'(x, y, t)$ is dominated by the turbulence and ϕ^* is dominated by nonturbulent submesoscale (<2 km) and mesoscale (>2 km) variations, both of which are common in the current dataset. Since stationary mesoscale motions are not obvious from repeated horizontal flight legs, we will collectively refer to the submesoscale and mesoscale motions as ''nonstationary motions.''

Analysis of aircraft slant soundings implicitly neglects $\phi^*(x, y, z, t)$ and assumes that the remaining nonturbulent part, $[\phi]$, can be estimated by an average along the slant sounding over horizontal distance L_{ave}, symbolized here as $\langle\phi(x, y, z, t)\rangle$. That is, the influence of horizontal variations of the nonturbulent part is neglected, and all nonturbulent variations are assumed to be part of the large-scale profile. Therefore, the flow is decomposed as

$$\phi(x,y,z,t) \equiv \langle\phi(z)\rangle + \phi'(x,y,t). \quad (2)$$

Turbulent fluctuations are then computed as deviations from $\langle\phi(x, y, z, t)\rangle$. This decomposition provides an estimate of the turbulent flux as $\langle w'\phi'\rangle$. Notice that this estimate of the turbulent fluctuations computed from averages along the aircraft slant soundings may be different from the theoretical definition in Eq. (1).

b. The error in the vertical mean gradient

The error in the estimated vertical gradient from the slant sounding that is due to horizontal gradients is $A^{-1}\partial\phi^*/\partial x$, where A is the ascent rate. The relative error that is due to horizontal gradients can be written as

$$\frac{\partial\phi^*}{\partial x}\Big/\frac{A\partial[\phi]}{\partial z}. \quad (3)$$

Errors in estimates of the vertical gradient are large if the horizontal gradients are not substantially smaller than the vertical gradient and if the ascent rate A is small. Over the 10-km horizontal flight tracks, the horizontal gradients of air temperature for the current data are normally too small to estimate. Horizontal gradients of the wind components, however, can be as large as $2 \times 10^{-4}\,\text{s}^{-1}$, which translates to a fictitious vertical gradient along the slant sounding of approximately $1.5 \times 10^{-3}\,\text{s}^{-1}$. This value corresponds, for example, to a fictitious difference of $1.5\,\text{m s}^{-1}$ over a 1-km segment of the sounding (75-m vertical distance).

This contamination of the estimated vertical gradient by horizontal gradients on the 10-km scale appears to be relatively unimportant with respect to the bulk vertical structure of the jet. On the submesohorizontal scale (< 2 km, corresponding to < 15 m vertical scale), the horizontal gradients and fictitious vertical gradients can be an order of magnitude larger (Fig. 9, described below in section 6) so that small-scale variations of the wind along the slant soundings do not necessarily represent mean vertical structure. We forego the temptation to smooth the soundings but note that small wiggles in the sounding probably do not represent true vertical structure.

c. Contamination of perturbation quantities by the mean vertical gradient

An aircraft ascent of δz leads to a change in ϕ of

$$\delta z\frac{\partial[\phi]}{\partial z} = \delta x A\frac{\partial[\phi]}{\partial z}, \quad (4)$$

where A is again the ascent rate. Choosing δx to be the averaging width L_{ave}, we estimate the relative error in ϕ' due to mean vertical variation captured within the averaging window as

$$L_{\text{ave}}A\frac{\partial[\phi]}{\partial z}\Big/\sigma_\phi, \quad (5)$$

where the standard deviation σ_ϕ is computed over the averaging window L_{ave}. We have assumed that the estimate of the mean vertical gradient is adequate. Whereas the error in the mean vertical gradient [Eq. (3)] is inversely related to the ascent rate, the error in the estimated turbulent fluctuations is proportional to the ascent rate.

If we define a vertical displacement or mixing length as

$$d \equiv \sigma_\phi\Big/\frac{\partial[\phi]}{\partial z},$$

then the relative error reduces to

$$\frac{AL_{\text{ave}}}{d} = \frac{\delta z}{d}, \tag{6}$$

where δz is the vertical climb over distance L_{ave}. This error is small if L_{ave} is chosen to be sufficiently small that δz is much smaller than d. It may be that choosing L_{ave} to be sufficiently small to control this error inadvertently removes important horizontal scales of turbulent fluctuations on horizontal scales greater than d/A. The ratio of the vertical scale to the horizontal scale of the turbulence is expected to be inversely related to the stratification so that the relative error in the turbulence increases with increasing stratification.

In terms of Eq. (5), the relative error is significant when vertical gradients are large and turbulent fluctuations are weak. For the more stable conditions (northern site; section 4), $\partial[\theta]/\partial z$ is estimated to be $0.075\,\text{K}\,\text{m}^{-1}$, corresponding to a vertical change of θ of 0.56 K over a 7.5-m change of height across an averaging window of 100 m. Here, θ is the potential temperature. Meanwhile, the observed standard deviation σ_θ is roughly 0.1 K. It is clear that the estimated σ_θ computed from the fluctuations within the averaging window L_{ave} is seriously contaminated by the vertical gradient of potential temperature. Because of potentially large relative errors, σ_θ and $w'\theta'$ cannot be confidently estimated from aircraft soundings. Estimating the momentum flux is hampered by similar uncertainties.

The corresponding error contribution to the vertical velocity fluctuations w' due to the height dependence of the mean vertical velocity appears to be much less important in comparison with that for temperature because of insignificant systematic vertical variation of $[w]$. The issue becomes somewhat ambiguous with gravity waves in the stable boundary layer where the horizontal and vertical variations of wave-induced w cannot be separated using slant soundings. Variations of w due to gravity waves may significantly contaminate the estimated standard deviation of vertical velocity σ_w, especially in cases of weak turbulence.

The above expectations are consistent with large disagreements between fluxes computed from level flight legs and fluxes computed from slant soundings. The variance $\overline{w'^2}$ computed from aircraft slant soundings seems to compare more favorably to those values from horizontal legs and will be used as a measure of the turbulent activity.

d. Choice of averaging window

For calculating the mean and the fluctuations about the mean, we choose a 100-m moving-averaging window along the slant sounding. A smaller averaging window would inadvertently increase the contribution of the turbulent fluctuations to the computed mean shear, especially for the more turbulent weakly stable case on 7 August. A larger averaging window would lead to more serious contamination of the fluctuations by the mean vertical gradient, particularly for the more stable conditions of 8 August. Then, deviations from the 100-m window might include significant nonturbulent motions, leading to overestimation of σ_w. At the same time, for thin, more stable boundary layers, the turbulence may have decreased substantially between the surface and the horizontal legs at 10 m or the lowest level of the sounding (Mahrt et al. 1998; Fairall et al. 2006), which would lead to underestimates of σ_w.

e. Gridded data

Some analyses will be based on gridded data computed by interpolating the instantaneous data to fixed levels vertically separated by 5 m. These gridded data will allow between-sounding analysis. Prior to the interpolation, no smoothing or averaging is applied to temperature or to the horizontal wind components. The standard deviation σ_w is computed from 100-m moving averages along the slant sounding and then interpolated to the grid levels.

f. Between-sounding analysis

We composited the gridded soundings during a given flight at the same general location as an estimate of mean vertical structure. The soundings cannot be considered as an ensemble because they are too few and the flow is not completely stationary. Using data interpolated to a vertical grid, we partition the flow at a given grid height as

$$\phi(x, y, z, t) \equiv [\phi](z) + \phi'(x, y, t). \tag{7}$$

Here $[\phi](z)$ is the average at a fixed level over all of the soundings and $\phi'(x, y, t)$ is the deviation of an individual sounding from the average over all of the soundings. Because the horizontal wind and temperature are instantaneous and are not preaveraged, $\phi'(x, y, t)$ includes turbulent fluctuations and nonstationary nonturbulent motions. Synoptic-scale changes and diurnal trends appear to be small during all three flights.

The between-sounding standard deviation $(\langle\phi'^2\rangle)^{1/2}$ is a measure of the nonstationarity, where here the angle brackets identify averaging over all of the soundings at a fixed level. The standard deviation of the between-sounding wind speed will be scaled by the wind speed averaged over all of the soundings. The between-sounding standard deviation of σ_w will be scaled by averaged

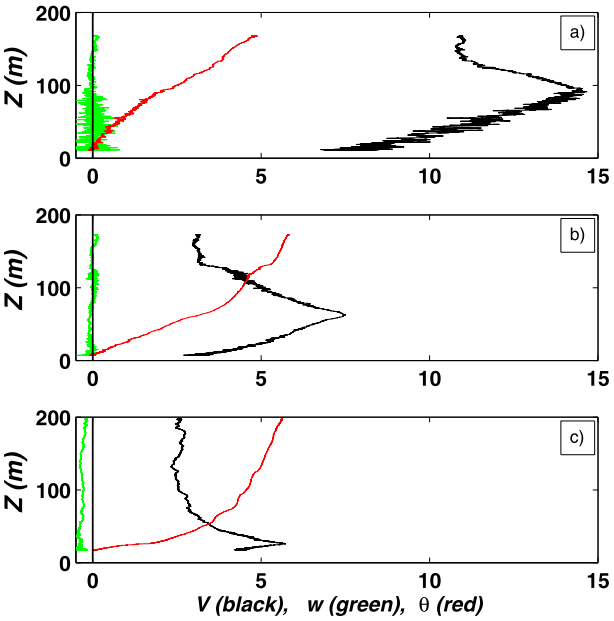

FIG. 3. An example of the vertical structure for (a) the weakly stable regime on 7 Aug, (b) the moderately stable regime at the southern site on 8 Aug, and (c) the very stable regime at the northern site on 8 Aug. Shown are wind speed V (black; m s^{-1}), mean potential temperature θ (red; K), and the standard deviation of vertical velocity w (green; m s^{-1}). Potential temperature is the deviation from the value at the lowest level.

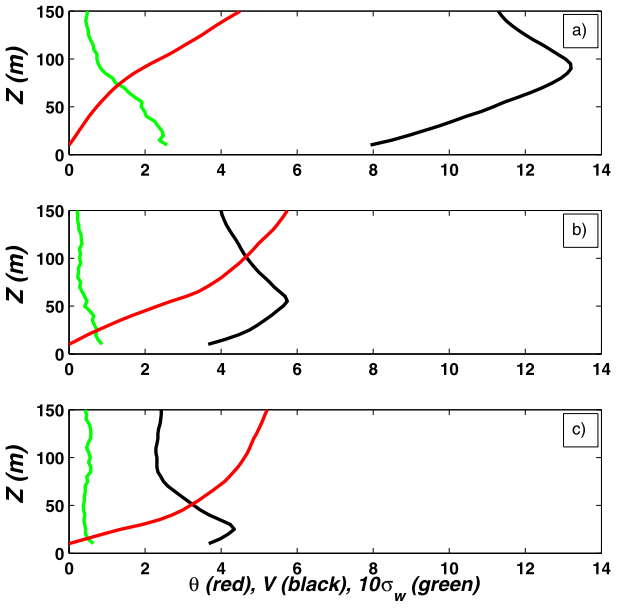

FIG. 4. Grid-interpolated values composited over the soundings: (a) the weakly stable regime on 7 Aug, (b) the moderately stable regime at the southern site on 8 Aug, and (c) the very stable regime at the northern site on 8 Aug. Shown are composited wind speed V (black; m s^{-1}), potential temperature θ (red; K), and $10 \times \sigma_w$ (green; m s^{-1}). Potential temperature is the deviation from the value at the lowest level.

value $\langle \sigma_w \rangle$. The relative standard deviation can then be written as

$$\hat{\phi} \equiv \langle \phi'^2 \rangle^{1/2} / \langle \phi \rangle , \tag{8}$$

which will be evaluated in section 6 where ϕ is the potential temperature, wind speed, or σ_w. The between-sounding standard deviation of the temperature will be scaled by the square of the averaged difference of potential temperature between 10 and 150 m.

4. Influence of stability and distance offshore

a. The three regimes

We now contrast the vertical structure of the marine boundary layer among the different stability regimes. Figure 3 shows examples of vertical structure from the weakly stable regime on 7 August, the moderately stable regime on 8 August, and the very stable regime on 8 August. Recall that the very stable group corresponds to the northern site closer to land as compared with the moderately stable group of soundings at the southern site. Each group of soundings is composited from the gridded data (section 3). In general, the composited profiles (Fig. 4) reveal a smoothed version of the individual profiles.

b. Vertical structure

The weakly stable regime (Figs. 3a and 4a) is associated with surface flow from the south-southwest, which advects air from warmer water. A well-defined wind maximum occurs at about 100 m and caps a partially mixed boundary layer where the stratification is modest. For some of the individual soundings on 7 August, the low-level wind maxima are less sharp than in Fig. 3a. The flow above the wind maximum is more significantly stratified, suggesting a diffuse capping inversion. The turbulence σ_w in the boundary layer below the wind maximum decreases systematically with height and is much smaller above the wind maximum, consistent with the usual concept of a well-defined boundary layer.

The surface wind for the moderately stable regime on 8 August (Figs. 3b and 4b) is from the west-southwest near the surface, rotates to westerly at 20 m, and is northwesterly at 150 m. This flow advects warmer air from land over cooler water, although the surface trajectory from land is longer than that at the jet height. Wind directional shear is a common complication in the coastal zone. In comparison with the weakly stable regime, the jet is sharper, the stratification near the surface is substantially stronger, and the height of the low-level wind maximum is lower—about 50 m as compared with nearly 100 m for the weakly stable regime.

The composited flow (Fig. 4b) in the moderately stable regime is characterized by strong stratification at the surface. The stratification decreases with height, in contrast to the weakly stable case. The strong stratification near the surface presumably results partly from the sharp decrease of surface temperature and surface roughness at the coastline and the subsequent feedback loops described in Fig. 1. The turbulence in the moderately stable boundary layer below the wind maximum is much weaker than for the weakly stable regime but decreases with height as in a traditional boundary layer.

Relative to the moderately stable regime at the southern site, the inversion layer at the northern site is thinner and the wind maximum is lower (Figs. 3c and 4c), averaging about 20 m above the sea surface. The stratification is even stronger than at the southern site. The very weak turbulence does not decrease systematically with height as in a traditional turbulent boundary layer. These features define the very stable regime. The wind direction for this very stable regime is from the west-southwest in the lowest 20 m and rotates with height toward the west-northwest at 150 m.

The small southerly wind component confined to near the surface at both sites might be a shallow onshore component driven by heating over land as part of the baroclinic contribution to the surface pressure. The wind directional shear is also in the same direction as Ekman turning, although such significant turning over a thin layer over the water has not been previously documented as Ekman rotation.

c. *Horizontal structure*

The observations for the very stable regime are characterized by mean sinking motion of several centimeters per second. Although the accuracy of mean vertical motion from aircraft measurements is uncertain, such sinking motion implies divergence and horizontal acceleration. The very stable regime is closer to the coast at the northerly site and is characterized by a thinner boundary layer and weaker low-level wind maxima in comparison with the moderately stable regime farther offshore at the southerly site. It is evident that the flow accelerates downwind, consistent with the observed subsidence, and the internal boundary layer thickens downwind as it grows by entrainment. The flows at the two sites are not on the same trajectory, however, and definite conclusions on growth of an internal boundary layer are not possible.

On the basis of the northwesterly wind direction at the height of the wind maximum at the southern site, the upwind distance to the heated land surface is roughly estimated to be 100 km. Using a jet speed of 6 m s^{-1}, we estimate that the flow from land would require about 4.5–5 h to reach the southern site. The spatial information is inadequate to perform a true upwind trajectory analysis, however, particularly with the irregular coastline and significant vertical rotation of the wind vector with height.

The very stable regime at the northern site is much closer to land. The wind is a little weaker, however, about 4.5 m s^{-1} at the jet height (Fig. 4), and the flow at the wind maximum is directed more from the west-northwest such that the angle between the flow and the coastline is smaller relative to the angle for the southern site. This smaller angle makes estimating the trajectory distance to the coast and the travel time more difficult. It appears that the trajectory distance to the upwind land surface at the height of the wind maximum is roughly 60–70 km, with a travel time of about 4 h.

For both the moderately stable regime at the southern site and the very stable regime at the northern site, the air temperature at 10 m is about 3–3.5 K higher than the SST. The temperature above the low-level wind maximum increases with time, consistent with advection from the heated land surface. This warming is much weaker than that over land, however, suggesting that at least intermittent mixing cools the advected warm air even above the wind maximum. Using soundings at the northern and southern sites for approximately the same period indicates that the temperature in the 20–60-m layer is 1–2 K higher at the northern site than at the southern site, probably due to more upward mixing of cold air and longer travel time enroute to the southern site.

Horizontal flight legs were flown at both the southern and northern sites, typically 30 km long and 10–15 m above the sea surface. The majority of the horizontal flight legs are perpendicular to the wind direction and do not reveal significant horizontal trends in air temperature and wind vector. Even flights parallel to the wind direction failed to depict significant systematic spatial variation. The horizontal variations are expected to be larger closer to the coast.

d. *Sharpness of the wind maxima*

The low-level wind maxima are often very sharp for the moderately stable and very stable regimes (Figs. 3b,c). Sharp marine jets have been reported previously. King et al. (2008) found a remarkably sharp low-level wind maximum in warm-air advection over a cooler ice shelf. Beardsley et al. (1987) and Winant et al. (1988) argued that the net influence of baroclinity and stress divergence is probably responsible for the well-defined sharp jets in their observations in the coastal zone. In their case, the thermal wind led to maximum geostrophic flow at the surface, but the maximum wind is

displaced upward because of the influence of stress divergence near the surface.

One might expect the very sharp jets to be dynamically unstable. Within the moderately stable and very stable regimes, the sharpness of the jet is poorly correlated to the strength of the turbulence. Short-term variations of jet sharpness appear to be out of phase with the turbulence. Sharper jets apparently produce shear-driven turbulence and diffusive smoothing of the jet followed by turbulence decay, resharpening of the jet, and so forth. Most low-level wind maxima are characterized by inflection points above the wind maxima. Inflection-point instability may contribute to the observed turbulence above the wind maxima, although definite conclusions would require three-dimensional information.

5. Surface fluxes and partial decoupling

On the basis of 30 horizontal legs for the weakly stable case, the surface friction velocity averages 0.21 m s^{-1} and z/L at the 10-m flight level averages 0.08, indicative of weakly stable conditions, where L is the measured Obukhov length. From 11 horizontal legs at 10 m for the moderately stable case at the southern site, the surface friction velocity averages only 0.08 m s^{-1} and the stability z/L increases to 0.26. For the very stable northern site, the 10-m horizontal flight legs are halfway to the wind maximum at 20 m and surface fluxes cannot be adequately estimated.

The gradient Richardson number computed between the bottom of the composited profile (10 m) and the height of the wind maximum is 1.2 at the very stable northern site but decreases to 0.47 at the moderately stable southern site, suggesting that the northern site is indeed more stable. The 10-m surface friction velocity computed from the horizontal legs intermittently decreases to 0.02–0.03 m s^{-1} at both sites. These very small values are comparable to those in the semidecoupled regime of Smedman et al. (1995) and Mahrt et al. (2001b).

Grisogono et al. (2007) and Grisogono and Rajak (2009) partitioned the turbulence associated with a low-level wind maximum into two regimes. When the height of the low-level wind maximum z_j is large relative to the Obukhov length, Monin–Obukhov similarity can potentially describe the behavior of the turbulence near the surface. When z_j is smaller than the Obukhov length, then z_j becomes a dominant length scale for describing the turbulence in the surface layer. Thus, Monin–Obukhov similarity theory can apply only when z_j/L is large and a traditional surface layer can be maintained. Even then, the jet may suppress large eddies and similarity theory may be invalidated (Smedman et al. 1995, 1997b).

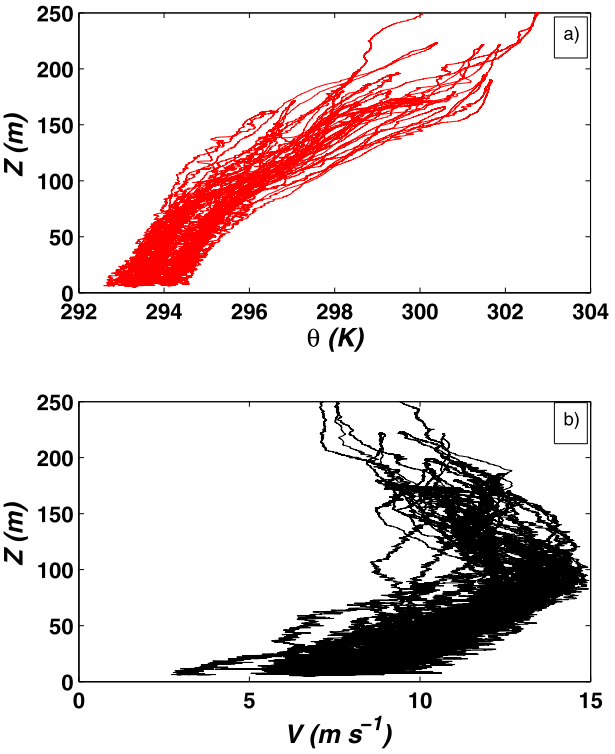

FIG. 5. Individual profiles of (a) potential temperature and (b) wind speed for the weakly stable regime on 7 Aug.

The ratio z_j/L for the weakly stable regime on 7 August and for the moderately stable regime at the southern site on 8 August is close to unity. Thus, Monin–Obukhov similarity does not apply, yet z_j is not a dominating length scale. This situation corresponds to an intermediate regime governed by multiple vertical length scales.

6. Nonstationarity

Pichugina et al. (2012) document strong time and space variability of low-level jets in the coastal zone. How representative is an individual sounding, and how nonstationary are the low-level profiles in the current data? Variability among the soundings is due to turbulence and nonstationary nonturbulent motions in addition to weak trends on the diurnal and synoptic scales. Despite considerable variability among soundings, the basic structure of the boundary layer and low-level wind maxima are relatively persistent for all three regimes (Figs. 5–7).

a. Wavelike variations

The speed and height of the wind maxima vary among soundings, but no trend in the height of the wind maxima within each group of soundings is detectable (Fig. 8). Only weak trends are detectable in the wind speed.

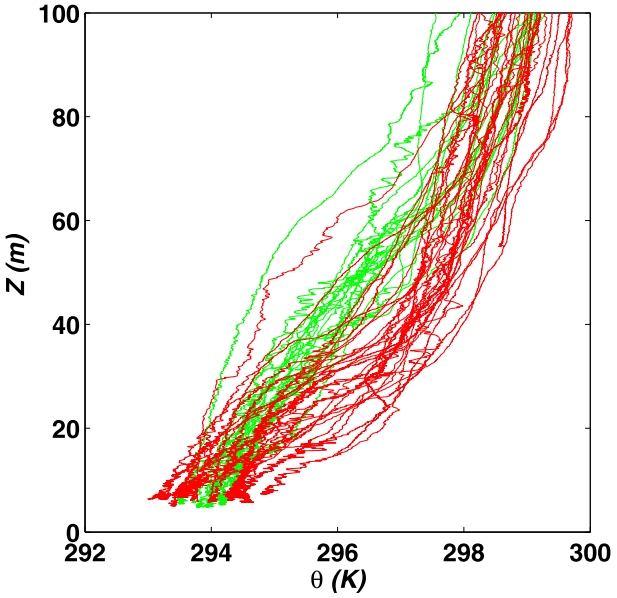

FIG. 6. Individual profiles of potential temperature on 8 Aug for the moderately stable regime at the southern site (green) and the very stable regime at the northern site (red).

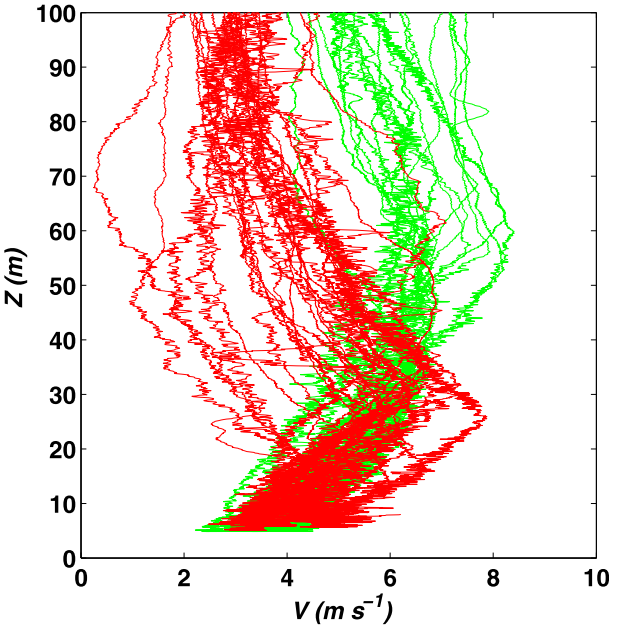

FIG. 7. As in Fig. 6, but for wind speed.

Low-level wind maxima are well defined for almost all of the soundings. Short-term variations, rather than trend, dominate the between-sounding variation. For the very stable regime at the northern site, the wind above the low-level wind maximum is relatively weak and especially variable (Fig. 7).

Some of the short-term variability in the vertical structure might be due to wavelike motions that are frequently observed from the horizontal aircraft legs. One of the best examples of a long train of wavelike motions is shown in Fig. 9, where the wavelength is a little less than a kilometer. This degree of wave organization occurred on only 2 of the 35 horizontal flight legs on 8 August. Subperiods of such wavelike motion characterized many of the other flight legs.

The spatial information from the aircraft might better reveal wavelike motions in comparison with the usual time series from fixed towers over land because the scale of the waves is better separated from the turbulence in the space domain than in the time domain. The better-defined wave activity over the sea might also be due to the simpler surface conditions over the sea. Over land, surface heterogeneity, obstacles, and topography can generate a variety of propagating, interfering wave motions that occur simultaneously with microfronts and more complex submesoscale motions (Belušić and Mahrt 2012; Mahrt et al. 2012).

For these data, the wavelike motions are characterized by a positive correlation between the westerly flow component and the temperature (Fig. 9). The absence of wavelike motions in the northerly component suggests oscillations that are confined primarily to the x–z plane. The plane of oscillation can have any orientation with respect to the wind direction. The relationship of the periodic temperature and u component with the vertical

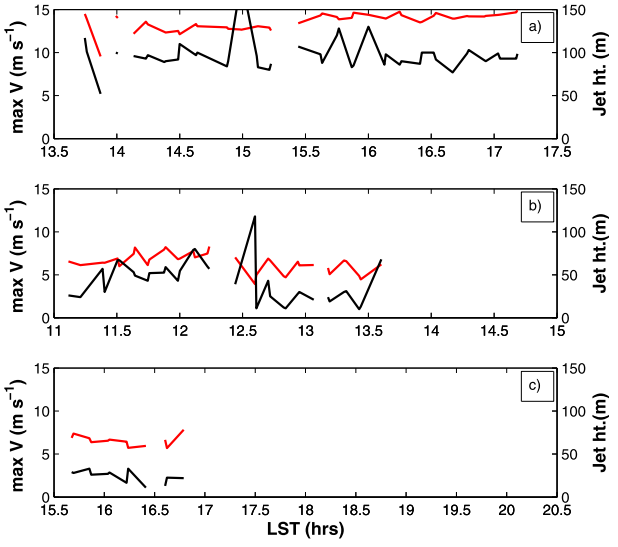

FIG. 8. Height (black) and speed (red) of the wind maximum for (a) the weakly stable regime on 7 Aug, (b) the moderately stable regime at the southern site on 8 Aug, and (c) the very stable regime at the northern site on 8 Aug. The isolated cases of significantly higher-level wind maxima correspond to poorly formed low-level wind maxima and could be classified as cases with no low-level wind maximum. LST is local standard time.

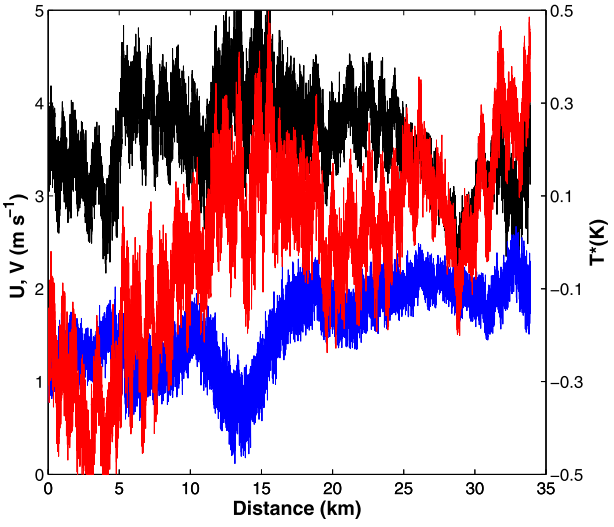

FIG. 9. The u component (black), the v component (blue), and the temperature deviation from the leg-averaged value (red) for horizontal leg 4 directed to the northwest from the southerly site in the moderately stable regime on 8 Aug.

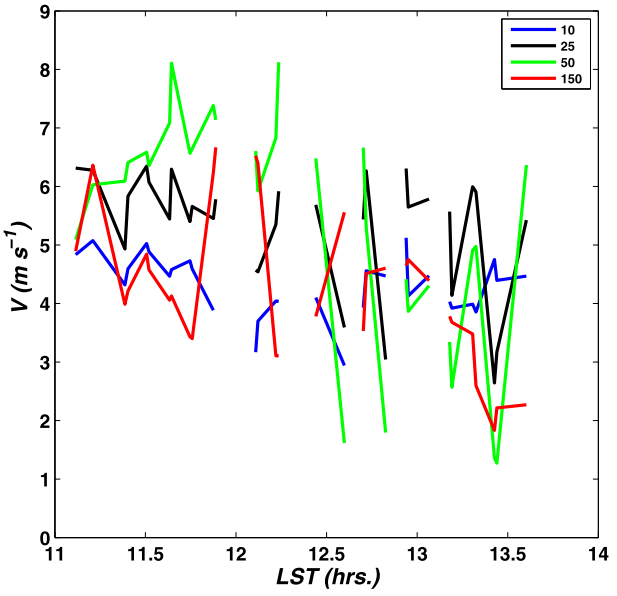

FIG. 10. Wind speed interpolated to fixed levels (10 m: blue; 25 m: black; 50 m: green; 150 m: red) for each of the soundings during the morning flight on 8 Aug. The soundings shifted northward at about 12.3 h. Gaps result when soundings did not satisfy the requirements on vertical extent (section 2).

motion is less defined. The height of the observations is close to the surface such that the signal of the wave vertical motion might be partially masked by the turbulence fluctuations. The wavelike motions in Fig. 9 are modulated by variability on the 5–10-km scale. Simultaneous variations on multiple scales occurred over all of the flight legs.

The short-term variations of the wind profile are now visualized in terms of the wind projected to fixed levels for each sounding (Fig. 10) and plotted for the entire morning flight of 8 August. At about 12.3 h in Fig. 10, the flight shifted from the southern site to the northern site (section 2), but the amplitude of the short-term variability remains about the same. For all four of the selected levels (10, 25, 50, and 150 m) for both the moderately stable and very stable regimes, the variation of the wind speed between soundings is a significant fraction of the mean speed and is greater than the trend in speed within both the moderately stable and very stable regimes. With the exception of one or two events, the short-term time changes are not coherent among levels. The generally poor vertical coherence leads to large time variations of the speed shear. This small vertical coherence argues against deep shear instability of the jet and instead points to the influence of shallow, nonstationary motions. Only one sounding on 8 August indicated a temperature reversal with height and implied overturning over a depth of more than a few meters.

b. Between-sounding variance

To quantify the between-sounding variations, we have evaluated the scaled between-sounding standard deviation defined in section 3. For the weakly stable regime (Fig. 11a), the scaled standard deviations for temperature, wind, and turbulence all increase with height. The wind is substantially more variable than potential temperature, largely because of small-scale nonstationary variations of wind rather than trend. As a result, an individual sounding may represent the mean bulk stratification but not necessarily represent the local mean shear.

For the moderately stable regime (Fig. 11b), the relative variability of the temperature reaches a maximum at or above the wind maximum. The scaled between-sounding standard deviation of wind speed reaches a local maximum around 50 m for the moderately stable regime and 30 m for the very stable regime, probably resulting from the variability of the height and speed of the low-level jet. In contrast to the weakly stable regime, the relative variability of the turbulence in the moderately and very stable regimes (Figs. 11b,c) is greater than the variability of the wind. With stronger stability, the turbulence is more intermittent or event-like, although it never completely vanishes.

7. Dynamics

Determining the cause of the low-level wind maxima is difficult because we have no information on the

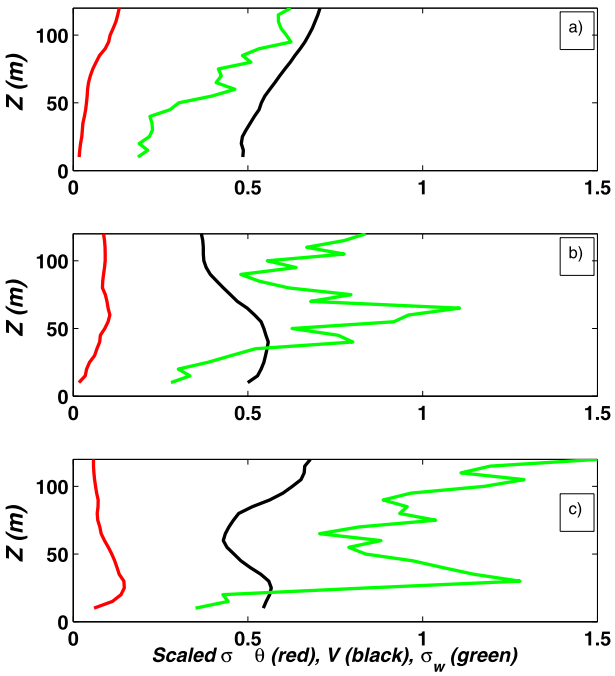

FIG. 11. Between-sounding standard deviation of V ($\mathrm{m\,s^{-1}}$) and σ_w ($\mathrm{m\,s^{-1}}$), each scaled by their mean value [Eq. (8)], and the between-sounding standard deviation of the temperature (K), scaled by the averaged vertical temperature difference, between 10 and 150 m for (a) the weakly stable regime on 7 Aug, (b) the moderately stable regime at the southerly site on 8 Aug, and (c) the very stable regime at the northern site on 8 Aug.

three-dimensional pressure field. In addition, the upwind conditions are complex because of islands and an irregular coastline. Significant rotation of the wind vector with height on the second day implies height-dependent origins of the air with respect to the coastline. It is most likely that the wind maxima reflect multiple causes. Numerical simulations currently under investigation significantly disagree with the observed winds at some locations. As a result, such simulations cannot be confidently used to extend the spatial variations of the wind over a larger domain. The following brief speculation is a plausibility exercise. We first consider the baroclinic influence and then the inertial mode.

a. *Baroclinic influence*

Satellite Advanced Very High Resolution Radiometer measurements of SST, aircraft measurements of SST and air temperature, and Weather Research and Forecasting model numerical simulations of air temperature all suggest warmer air to the north, west, and southwest of the observational domain with cooler air to the east and northeast. The contribution of the low-level horizontal temperature gradient to the horizontal gradient of hydrostatic pressure at the surface is approximately (Dutton 1986; Mahrt et al. 2004)

$$\alpha_o \nabla_H P_b \approx -\frac{g h_T}{\Theta_o} \nabla_H [\theta]. \tag{9}$$

Here P_b is the contribution of the low-level baroclinity (thermal wind) between the surface and height h_T, ideally chosen to be just above the level of significant surface-based $\nabla_H[\theta]$, $[\theta]$ is the averaged potential temperature from the surface up to h_T; and Θ_o and α_o are scale values of the potential temperature and specific volume, respectively. This baroclinity most effectively generates low-level wind maxima when the horizontal temperature gradient decreases with height, as occurs with horizontal temperature gradients associated with heterogeneous surface heating.

A combination of observations and numerical results suggests a horizontal gradient of air temperature in the lowest 100 m that is on the order of $10^{-4}\,\mathrm{K\,m^{-1}}$ between the coast and the two observational sites. This estimate is a maximum value since the strongest horizontal temperature gradient is expected close to the coast where the depth of the horizontal temperature gradient is thin. These values correspond to a baroclinic contribution to the surface pressure gradient on the order of $3 \times 10^{-4}\,\mathrm{m\,s^{-2}}$, equivalent to a geostrophic wind of $3\,\mathrm{m\,s^{-1}}$. At the observational sites, the horizontal gradient of the vertically averaged potential temperature appears to result more from an increase in the depth of the cold air than from the horizontal gradient of temperature within the cold air. This baroclinic contribution to the horizontal pressure gradient would act to oppose the flow. Since the wind maxima do form, the baroclinic mode must be smaller than the mechanism responsible for formation of the low-level wind maxima. Again, these estimates are based on combining observations with limited spatial domain and numerical results and could be contaminated by large errors.

b. *Inertial mode*

The airflow crossing the coastline from the heated land surface over the cooler water corresponds to warm-air advection and creates stable stratification near the surface. The decrease of surface roughness acts to accelerate the flow. These mechanisms act in concert through feedback mechanisms sketched in Fig. 1. The resulting upset of the force balance leads to an inertial mode. An inertial mode may develop above the thin stable boundary layer over the cool water. The solution for an idealized pure inertial mode for constant geostrophic wind $\mathbf{V}_g$ (Garratt 1992) is

$$\mathbf{V}_H = [\mathbf{V}_H(t=0) - \mathbf{V}_g]\exp(-ift) + \mathbf{V}_g, \qquad (10)$$

where t is Lagrangian time following the flow from the initial collapse. With an assumed instantaneous collapse of the mixed layer and a height-independent geostrophic wind, the ageostrophic flow and the inertial mode are independent of height over the depth of the well-mixed part of the previous convective boundary layer.

Although this height-independent behavior is well produced in numerical models, it is not generally observed. In fact, low-level wind maxima form. Mahrt (1981) argued that during the evening transition over land the stress divergence evolves over a finite time, producing a height-dependent ageostrophic flow with a maximum. It is unlikely that Mahrt's explanation alone can explain the strength and sharpness of the jets observed in this study, however. Van de Wiel et al. (2010) derived a height-dependent, frictionally modified inertial oscillation about an equilibrium boundary layer wind that may offer more potential. Explicit application of this concept to the current data requires more reliable information on the pressure field, however.

The baroclinic mode, which decreases with height, acts to decelerate the near-surface wind and to enhance the shear on the underside of the jet, which may contribute to the sharpness of the jet. In addition to the influence of inertial and baroclinic modes, the low-level wind may also be influenced by intermittent turbulent mixing near and above the wind maxima, small-scale transient motions, and jet-induced pressure adjustments resulting from horizontal divergence and convergence in a stratified environment. The data are inadequate for separating this potentially complex set of mechanisms that influence the wind maxima.

8. Conclusions

The Long-EZ aircraft flew 102 low-level slant soundings off the northeast coast of the United States on two summer days. The first day is characterized by a weakly stable boundary layer capped by an inversion. Relatively strong jet speeds of 10–15 m s^{-1} occur at the top of the weakly stable boundary layer at about 100 m. The second day is characterized by weaker jet speeds on the order of 5 m s^{-1} and stronger stability due to advection of warm air from land. The height of the wind maximum is lower, averaging 50 m for the moderately stable regime at the southern site farther from the coast and averaging 20 m for the very stable regime at the northern site closer to the coast. The wind maxima on this day are very sharp.

Fluxes computed from the aircraft soundings were not reported in this study because they are vulnerable to potentially serious errors (section 3), although the behavior of the vertical velocity variance could be evaluated. The relatively deeper (but still shallow) boundary layer and relatively stronger jet farther offshore are consistent with the concept of accelerating flow in a growing stable internal boundary layer downwind from the coast. The two sites are not on the same trajectory, however, and both sites include significant directional shear, precluding definite conclusions.

The low-level jet varies significantly between subsequent soundings on time scales of tens of minutes or less. This variability is generally coherent only over small depths. The negative speed shear above the wind maximum is large, and the turbulence at these levels can be significant for individual soundings. The relative variation of the wind and turbulence among the soundings is much greater than that for temperature. Nonetheless, the jet remains persistent within each observational period of several hours.

An attempt to assess the cause of the low-level wind maxima indicates that an inertial mode is probably important but by itself cannot explain the rapid formation of the wind maxima and their sharpness. The baroclinic mode acts to decelerate the flow near the surface, which could enhance the shear on the underside of the wind maximum and also induce wind directional shear. Our data were inadequate for isolation of these mechanisms, however. Helmis et al. (2013) showed that multiple simultaneous influences lead to low-level summer jets off the east coast of the United States. A complete evaluation of the equation of motion and the relative roles of baroclinic and inertial modes would require more information on the three-dimensional pressure field and continuous horizontal variation of the wind field. Because of the nonstationarity of the jet, a large number of soundings is also needed. Small, remotely controlled aircraft could more economically meet these needs. The potential greater flexibility of unmanned aircraft, including a steeper ascent rate, might reduce the potentially significant errors in the estimated mean vertical profile (section 3).

Acknowledgments. Very helpful comments from two reviewers, Branko Grisogono and Bas van den Wiel, are greatly appreciated. We also thank Sukanta Basu and Branko Kosovic for numerical simulations of 8 August 2001. This work was supported by the U.S. Office of Naval Research through Award N00014-11-1-0073. Mahrt was additionally supported by ONR Grant N00014-11-WX20724 and DOE Grant DE-EE0005373.

REFERENCES

Andreas, E. L, K. J. Claffey, and A. P. Makshtas, 2000: Low-level atmospheric jets and inversions over the western Weddell Sea. *Bound.-Layer Meteor.,* **97,** 459–486.

Angevine, W. M., M. Tjernström, and M. Žagar, 2006: Modeling of the coastal boundary layer and pollutant transport in New England. *Bound.-Layer Meteor.,* **45,** 137–154.

Beardsley, R. C., C. E. Dorman, C. A. Friehe, L. K. Rosenfeld, and C. D. Winant, 1987: Atmospheric forcing during the Coastal Ocean Dynamics Experiment: A description of the marine boundary layer and atmospheric conditions over a northern California upwelling region. *J. Geophys. Res.,* **92,** 1467–1468.

Belušić, D., and L. Mahrt, 2012: Is geometry more universal than physics in atmospheric boundary layer flow? *J. Geophys. Res.,* **117,** D09115, doi:10.1029/2011JD016987.

Bielli, F., P. Barbour, R. Samelson, E. Skyllingstad, and J. Wilczak, 2002: Study of the diurnal cycle along the central Oregon coast during summertime northerly flow. *Mon. Wea. Rev.,* **130,** 992–1008.

Burk, S. D., and W. T. Thompson, 1996: The summertime low-level jet and marine boundary layer structure along the California coast. *Mon. Wea. Rev.,* **124,** 668–686.

Colle, B. A., and D. R. Novak, 2010: The New York Bight jet: Climatology and dynamical evolution. *Mon. Wea. Rev.,* **138,** 2385–2404.

Crawford, T., and R. Dobosy, 1992: A sensitive fast-response probe to measure turbulence and heat flux from any airplane. *Bound.-Layer Meteor.,* **59,** 257–278.

Donelan, M. A., 1990: Air–sea interaction. *Ocean Engineering Science,* B. LeMehaute and D. M. Hanes, Eds., John Wiley and Sons, 239–292.

Dutton, J., 1986: *The Ceaseless Wind.* Dover, 671 pp.

Fairall, C. W., and Coauthors, 2006: Turbulent bulk transfer coefficients and ozone deposition velocity in the International Consortium for Atmospheric Research into Transport and Transformation. *J. Geophys. Res.,* **111,** D23S20, doi:10.1029/2006JD007597.

Garratt, J., 1992: *The Atmospheric Boundary Layer*. Cambridge University Press, 316 pp.

Grisogono, B., and Z. Rajak, 2009: Assessment of Monin–Obukhov scaling over small slopes. *Geofizika,* **26,** 101–108.

——, L. Ström, and M. Tjernström, 1998: Small-scale variability in the coastal atmospheric boundary layer. *Bound.-Layer Meteor.,* **88,** 23–46.

——, L. Kraljević, and J. Jeričević, 2007: The low-level katabatic jet height versus Monin–Obukhov height. *Quart. J. Roy. Meteor. Soc.,* **133,** 2133–2136.

Helmis, C., Q. Wang, G. Sgouros, S. Wang, and C. Halios, 2013: Investigating the summertime low-level jet over the east coast of the U.S.A. *Bound.-Layer Meteor.,* **149,** 259–276.

Högström, U., 1984: The wind regime in coastal areas with special reference to results obtained from the Swedish Wind Energy Program. *Bound.-Layer Meteor.,* **30,** 351–373.

Jiang, Q., S. Wang, and L. O. Neill, 2010: Some insights into the characteristics and dynamics of the Chilean low-level coastal jet. *Mon. Wea. Rev.,* **138,** 3185–3206.

King, J., T. A. Lachlan-Cope, R. S. Ladkin, and A. Weiss, 2008: Airborne measurements in the stable boundary layer over the Larsen Ice Shelf, Antarctica. *Bound.-Layer Meteor.,* **127,** 413–428.

Lange, B., S. Larsen, J. Højstrup, and R. Barthelmie, 2004: The influence of thermal effects on the wind speed profile of the coastal marine boundary layer. *Bound.-Layer Meteor.,* **122,** 587–617.

Lenschow, D. H., and J. Sun, 2007: The spectral composition of fluxes and variances over land and sea out to the mesoscale. *Bound.-Layer Meteor.,* **125,** 63–84.

Mahrt, L., 1981: The early evening boundary layer transition. *Quart. J. Roy. Meteor. Soc.,* **107,** 329–343.

——, D. Vickers, J. Edson, J. Sun, J. Højstrup, J. Hare, and J. M. Wilczak, 1998: Heat flux in the coastal zone. *Bound.-Layer Meteor.,* **86,** 421–446.

——, ——, ——, J. Wilczak, J. Hare, and J. Højstrup, 2001a: Vertical structure of turbulence in offshore flow during RASEX. *Bound.-Layer Meteor.,* **100,** 47–61.

——, ——, J. Sun, T. L. Crawford, G. Crescenti, and P. Frederickson, 2001b: Surface stress in offshore flow and quasi-frictional decoupling. *J. Geophys. Res.,* **106,** 20 629–20 639.

——, ——, and E. Moore, 2004: Flow adjustments across sea-surface temperature changes. *Bound.-Layer Meteor.,* **111,** 553–564.

——, S. Richardson, N. Seaman, and D. Stauffer, 2012: Turbulence in the nocturnal boundary layer with light and variable winds. *Quart. J. Roy. Meteor. Soc.,* **138,** 1430–1439.

Mayer, S., M. O. Jonassen, A. Sandvik, and J. Reuder, 2012: Profiling the Arctic stable boundary layer in Advent Valley, Svalbard: Measurements and simulations. *Bound.-Layer Meteor.,* **143,** 507–526.

Muñoz, R. C., and R. D. Garreaud, 2005: Dynamics of the low-level jet off the west coast of subtropical South America. *Mon. Wea. Rev.,* **133,** 109–132.

Nunalee, C. G., and S. Basu, 2013: Mesoscale modeling of coastal low-level jets: Implications for offshore wind resource estimation. *Wind Energy (Chichester Engl.),* **99,** 1–18.

Pichugina, Y. L., R. M. Banta, W. A. Brewer, S. P. Sandberg, and R. M. Hardesty, 2012: Doppler lidar–based wind-profile measurement system for offshore wind-energy and other marine boundary layer applications. *J. Appl. Meteor. Climatol.,* **51,** 327–349.

Rahn, D. A., and T. R. Parish, 2010: Cessation of the 22–25 June 2006 coastally trapped wind reversal. *J. Appl. Meteor. Climatol.,* **49,** 1412–1428.

Skyllingstad, E., R. Samelson, L. Mahrt, and P. Barbour, 2005: A numerical modeling study of warm offshore flow over cool water. *Mon. Wea. Rev.,* **133,** 345–361.

Smedman, A.-S., H. Tjernström, and U. Högström, 1993: Analysis of the turbulence structure of a marine low-level jet. *Bound.-Layer Meteor.,* **66,** 105–126.

——, H. Bergström, and U. Högström, 1995: Spectra, variances and length scales in a marine stable boundary layer dominated by a low level jet. *Bound.-Layer Meteor.,* **76,** 211–232.

——, ——, and B. Grisogono, 1997a: Evolution of stable internal boundary layers over a cold sea. *J. Geophys. Res.,* **102,** 1091–1099.

——, U. Högström, and H. Bergström, 1997b: The turbulence regime of a very stable marine airflow with quasi-frictional decoupling. *J. Geophys. Res.,* **102,** 21 049–21 059.

Ström, L., and M. Tjernström, 2004: Variability in the summertime coastal marine atmospheric boundary-layer off California, USA. *Quart. J. Roy. Meteor. Soc.,* **130,** 423–448.

Sun, J., D. Vandemark, L. Mahrt, D. Vickers, T. Crawford, and C. Vogel, 2001: Momentum transfer over the coastal zone. *J. Geophys. Res.,* **106,** 12 437–12 488.

Tastula, E.-M., T. Vihma, and E. L. Andreas, 2012: Evaluation of Polar WRF from modeling the atmospheric boundary layer

over Antarctic sea ice in autumn and winter. *Mon. Wea. Rev.,* **140,** 3919–3935.

Tjernström, M., and A.-S. Smedman, 1993: The vertical turbulence structure of the coastal marine atmospheric boundary layer. *J. Geophys. Res.,* **98,** 4809–4826.

van de Wiel, B. J. H., A. F. Moene, G. J. Steeneveld, P. Baas, F. C. Bosveld, and A. A. M. Holtslag, 2010: A conceptual view on inertial oscillations and nocturnal low-level jets. *J. Atmos. Sci.,* **67,** 2679–2689.

Vihma, T., J. Uotila, and J. Launiainen, 1998: Air–sea interaction over a thermal marine front in the Denmark Strait. *J. Geophys. Res.,* **103,** 27 655–27 678.

Winant, C. D., C. E. Dorman, C. A. Friehe, and R. C. Beardsley, 1988: The marine layer off northern California: An example of supercritical channel flow. *J. Atmos. Sci.,* **45,** 3588–3605.

Zemba, J., and C. A. Friehe, 1987: The marine atmospheric boundary layer jet in the Coastal Ocean Dynamics Experiment. *J. Geophys. Res.,* **92,** 1489–1496.